PCCP

Accepted Manuscript

ROYAL SOCIETY OF CHEMISTRY

www.rsc.org/pccp

PCCP

COMMUNICATION

NO adsorption and diffusion on hydroxylated rutile TiO_2(110)

Yan-Yan Yu [a], *Ulrike Diebold* [b], *Xue-Qing Gong* [a,*]

Received 00th January 20xx,
Accepted 00th January 20xx

DOI: 10.1039/x0xx00000x

www.rsc.org/

We report a computational study of NO adsorption and diffusion on the hydroxylated rutile TiO_2(110) surface performed with Density functional theory (DFT) calculations corrected by on-site Coulomb corrections and long-range dispersion interactions. NO prefers to adsorb with its N-end down at surface Ti_{5c} sites. The excess electron that is located at a subsurface site for the hydroxylated surface localizes in the 2π* orbital of the adsorbed NO. A novel 'roll-over' diffusion scheme is proposed that involves three neighboring Ti_{5c} atoms and one surface hydroxyl, with an O-end down NO at the middle Ti_{5c} as the intermediate state. During the migration, NO can also form bridging species between two Ti_{5c} atoms. The calculated scanning tunneling microscopy (STM) features with the "bright-dark-bright" configuration corresponding to diffusing NO at different positions are consistent with the experimental STM results.

In the past few decades, titanium dioxide has emerged as a promising material with numerous applications in diverse and technologically important areas such as heterogeneous catalysts, (photo-)electrodes, and gas sensors[1-4]. Moreover, the rutile TiO_2(110) surface, as the most stable facet of titanium dioxide, has evolved as a key model system to study fundamental surface properties and processes at the molecular level. It has been widely proposed that the surface physics and chemistry of TiO_2 is heavily influenced, and often even dominated, by surface defects such as O vacancies, Ti interstitials, surface hydroxyls and step edges[5]. In particular, much attention has been paid to intrinsic defects, such as surface O vacancies and, more recently, subsurface Ti interstitials, and how these may affect the adsorption of probe molecules such as O_2 or CO[6-14]. Another important type of defect at TiO_2 is a hydroxyl; in fact, it is believed that surface hydroxyls are active species in photocatalysis and photoinduced hydrophilicity[15-17], and Ti(OH) groups are supposed to be important surface traps for charge carriers, forming $Ti^{4+}(OH)^{\bullet}$ radicals (hole trapping) or Ti^{3+}(OH) groups (electron trapping)[15, 17]. On the other hand, surface processes involving small molecules such as CO and NO are also important since they are closely related to applications in vehicle emission control and other hazardous gas detection. Specifically, the catalytic reduction of nitric oxide (NO) from exhaust streams plays an important role in the control of air pollution and has drawn much attention recently[18, 19].

In our previous report[20], we used scanning tunneling microscopy (STM), X-ray/ultraviolet photoemission spectroscopy (XPS/UPS), and density functional theory (DFT) calculations to investigate this system. We found that NO interacts mainly with surface hydroxyls on rutile TiO_2(110), and is bound strongly enough to be stable at room temperature. Moreover, after dosing NO at 300 K STM images showed a new feature with a characteristic "bright-dark-bright" (BDB) contrast along the Ti_{5c}. The BDB features were assigned as NO-related, as their number of BDB, the NO exposure, and the OHs followed a 1:1:1 ratio. Interestingly, once a BDB appeared, a neighboring OH spot disappeared in the STM image, and conversely, when a BDB feature disappeared, a hydroxyl appeared on a neighboring O_{2c} site. From DFT calculations, we have demonstrated that surface hydroxyls may promote NO adsorption through charge transfer, which gives rise to a negatively charged NO^- and strong electrostatic interaction with surface Ti^{4+}. However, the origin of the BDB features in STM had remained unclear.

In this letter, we use DFT calculations to shed light on this phenomenon. NO adsorption at different, five-fold coordinated Ti surface atoms (Ti_{5c}) of rutile TiO_2(110) as well as NO diffusion are systematically calculated and compared. The electronic structures of the various key surface species including the intermediate states in the diffusion channels are

[a] *Key Laboratory for Advanced Materials, Centre for Computational Chemistry and Research Institute of Industrial Catalysis, East China University of Science and Technology, 130 Meilong Road, Shanghai 200237, People's Republic of China.* *E-mail: xgong@ecust.edu.cn*
[b] *Institute of Applied Physics, Vienna University of Technology, Wiedner Hauptstrasse 8-10/134, 1040 Vienna, Austria*

Electronic Supplementary Information (ESI) available: The electronic structure of hydroxylated rutile TiO2(110) and DOS of NO on the surface and NO diffusion pathway III. See DOI: 10.1039/x0xx00000x

taken into account for analysis. Furthermore, simulated STM images are obtained for comparison with the experimental ones. Our results suggest that the distinct diffusion behavior of NO is the origin of the BDB features.

The calculations were performed with the Vienna *ab initio* simulation package (VASP)[21, 22]. The exchange correlation was described by the Perdew, Burke, and Ernzerhof functional within the generalized gradient approximation (PBE-GGA)[23]. The project-augmented wave (PAW)[24, 25] method was used to represent the core-valence electron interaction. The calculations were also conducted involving on-site Coulomb corrections[26, 27] (DFT+U, U = 4.2 eV for Ti 3*d* states) and long-range dispersion interactions[28, 29] (DFT-D). The U value was chosen for it is suggested by Setvin *et al.*[30] that one needs a U of at least 3.8 eV to describe accurately the electron localization in DFT. The Ti *3s*, *3p*, 3d, *4s*, and the N and O *2s*, *2p* electrons were treated as valence electrons and an energy cutoff of 400 eV for the basis-set expansion was used. To investigate NO diffusion, the CI-NEB method was employed[31, 32]. The rutile TiO_2(110) surface was modeled as a periodic slab with five O-Ti-O trilayers of oxide, and the vacuum between slabs was >15 Å. A 6×2 surface cell and corresponding 1×1×1 k-point mesh were used in the calculations. The adsorption was modeled on one side of the slab, and during structural optimizations all of the atoms except those in the bottom TiO_2 trilayer of the slab were allowed to relax until atom forces reached < 0.05 eV/Å. To estimate the adsorption energy (E_{ads}) of NO, the following expression was considered:

$$E_{ads} = -[E_{NO/TiO_2} - E_{NO} - E_{TiO_2}]$$

where E_{NO/TiO_2} is the total energy of the interacting system containing NO molecule and TiO_2 support in a surface cell; E_{TiO_2} is the total energy of the rutile TiO_2(110) slab; and E_{NO} is the total energy of a single NO molecule in gas-phase.

The hydroxylated TiO_2(110) surfaces were modeled by adding one H atom to a two-fold coordinated ('bridge-bonded') surface O_{2c} (see Fig. S1(a)). In agreement with a previous study[33], one excess electron was located most stably at the first-neighbor subsurface Ti atom (see Fig. S1(b)); if the excess electron was trapped at different Ti_{5c} atoms on the surface (see Figs. S1(c)-(f)), the total energies were calculated to be ~0.2 eV higher. NO adsorption configurations on stoichiometric and hydroxylated rutile TiO_2(110) surfaces were calculated and the geometric and electronic structures are shown in Fig. 1. NO has an unpaired electron in its 2π* anti-bonding orbital, and it takes the N-down configuration at both the clean and hydroxylated surface. At the stoichiometric clean surface, NO is only physisorbed at the five-fold coordinated Ti (Ti_{5c}); the calculated adsorption energy of 0.53 eV is slightly higher compared to previous reports[34] (~0.4 eV), largely due to the fact that we have included long-range dispersion interactions in the present calculations. On the hydroxylated surface, the surface excess electron can transfer to the adsorbed NO (see Fig. 1(d)). The favorable electrostatic interaction between NO^- and Ti^{4+} results in stronger adsorption with a higher adsorption energy of 0.82 eV. An analysis of the electronic density of states in Figs. S2(a) and (b) also confirms that the excess electron is now localized at the adsorbed NO.

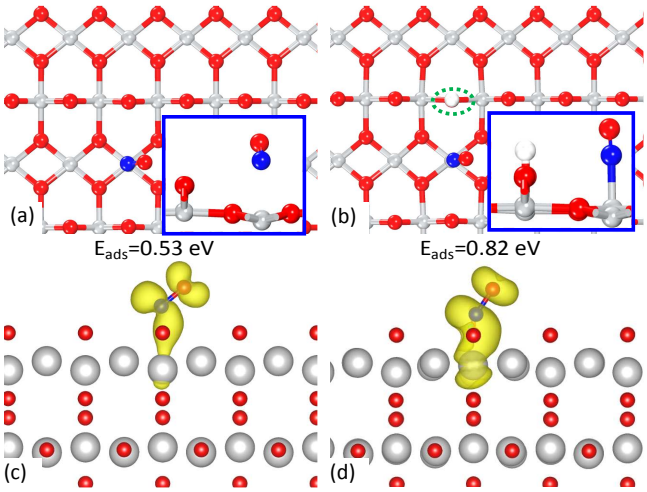

Fig. 1 Calculated structures of NO adsorbed on an (a) stoichiometric, and (b) hydroxylated rutile TiO_2(110) surface in top and side view (insets). The corresponding adsorption energies are listed. (c)-(d) Isosurfaces of calculated spin charge densities (yellow). N atoms are in blue, O in red, H in white and Ti in grey; the dotted ellipse in green shows the hydroxyl; these notations are used throughout this paper.

In a study by Hu and co-workers, O_2 adsorption on the Au/TiO_2(110) surface has been calculated[35]. They found that the effect of an OH group on O_2 adsorption is surprisingly long-ranged and that the O_2 adsorbed on the surface in the presence of OH can diffuse along the Ti_{5c} row of TiO_2(110). In addition, Ganesh *et al.*[36] has also found that the hydroxyls at rutile TiO_2(110) have a long range effect increasing the adhesion of gold clusters, and the induced charge transfer can enhance the molecular adsorption and coadsorption energies of CO and O_2 on the surface. Here we calculated NO adsorbed at different Ti_{5c} atoms on the hydroxylated rutile TiO_2(110) surface, and the calculated structures and adsorption energies are listed in Fig. 2. Similar to the previous work,[35, 36] our results also show that the effect of OH on NO adsorption is long-ranged, and that the adsorption energy differences are small for NO at the first-, second- and third-neighbor Ti_{5c} with respect to the hydroxyl. The calculated electronic structures (not shown) further illustrate that the adsorbed NO incorporates the excess electron in all cases. This is consistent with our results for the hydroxylated surface without the NO that shows negligible energy differences when the excess electron is trapped at different surface Ti_{5c} atoms (see Figs. S1(d)-(e)).

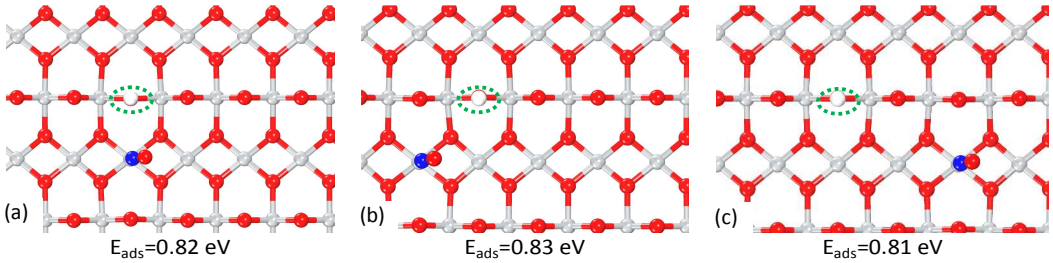

Fig. 2 Calculated structures (top view) of NO adsorbed at various Ti_{5c} atoms on the hydroxylated rutile TiO_2(110) surface. The corresponding adsorption energies are listed below.

We also calculated the diffusion of NO along the row of Ti_{5c} at TiO_2(110). Since the Ti_{5c} second-nearest to the hydroxyl is the most favorable site for NO adsorption, followed by the first-nearest one, and then the Ti atoms further away (see Fig. 2), we considered two diffusion pathways beginning with NO adsorbed at the second-nearest and first-nearest Ti_{5c}, respectively. The results are illustrated in Figs. 3 (Pathway I) and 4 (Pathway II), respectively. In both pathways, the NO migration involves three adjacent Ti_{5c} atoms ("left-middle-right"). In the intermediate states (IMS) the NO adsorbs with its O-end down at the middle Ti_{5c}. Before it reaches this IMS, the NO diffuses from the left Ti_{5c} with its O atom approaching the middle Ti_{5c}, forming a bridge species over the two Ti_{5c} ("left and middle"). Then, the adsorbed "ON" (O-end down) in the IMS can rotate around its Ti-O bond with an extremely small barrier (0.02 eV (Pathway I) and 0.06 eV (Pathway II)), and the N-end of NO approaches the right Ti_{5c} on the opposite side and forms a new bridge species over the two Ti_{5c} ("middle and right"). Finally, the adsorbed ON continues to move toward the right Ti_{5c} and binds in the favorable N-end down configuration. The overall barrier is 0.45 eV for Pathway I, and it is 0.50 eV for Pathway II. We also located a rather common diffusion pathway for NO with the N-end down all the way, and it gives the barrier of 0.75 eV (see Pathway III in Fig. S3), which is much higher than those of the "roll-over" processes (Pathways I&II). Thus, we propose that the "roll over" mechanism dominates the diffusion pathway for NO at hydroxylated rutile TiO_2(110).

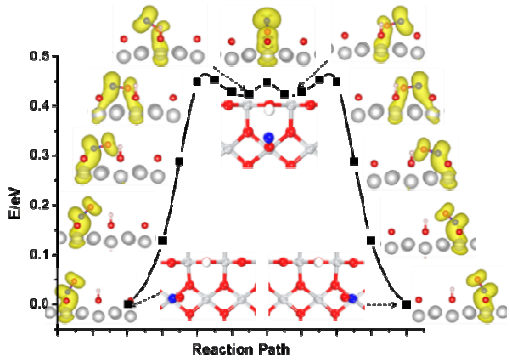

Fig. 3 Calculated energy profile of NO diffusion through Pathway I.

According to the analysis above, NO can adsorb and diffuse readily at the nearest few Ti_{5c} beside the hydroxyl of rutile TiO_2(110). Specifically, through Pathway I, NO can migrate from the left(right) second-nearest to first-nearest (middle) and then to right(left) second-nearest Ti_{5c}; and through Pathway II, from first-nearest to second-nearest and then to third-nearest one. The calculated energy profiles of the two pathways are quite similar. The overall barrier in Pathway II is slightly higher (~0.50 eV) than that in Pathway I (~0.45 eV), such values suggest that diffusivity is quite high at room temperature. However, for Pathway I (Fig. 3), the reaction process is completely symmetrical, while for Pathway II (see Fig. 4), it clearly becomes more and more difficult for NO to move further away from the first-nearest Ti_{5c}, indicating that NO may tend to stay at the neighboring sites of a surface hydroxyl. It should also be mentioned that the IMS in Pathway II is quite unstable, which is largely due to the absence of an H-bond with the hydroxyl, and
accordingly, the intermediate ON may desorb easily. Then, after it re-adsorbs at the favorable second-nearest Ti_{5c}, its diffusion may turn to follow the Pathway I. Thereby we expect that Pathway I (Fig. 3) is the most favorable one for NO to follow, and is also most likely to determine the appearance STM features of NO in experimental work.

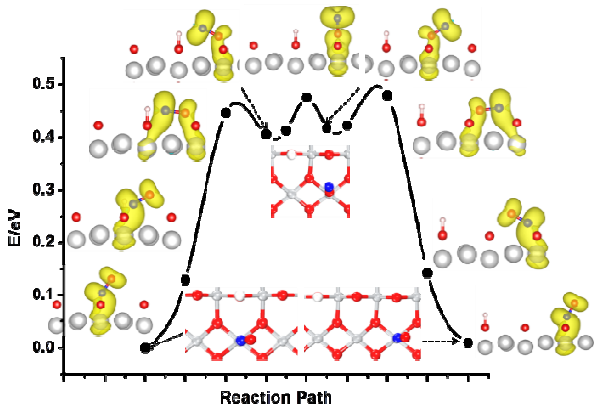

Fig. 4 Calculated energy profile of NO diffusion through Pathway II.

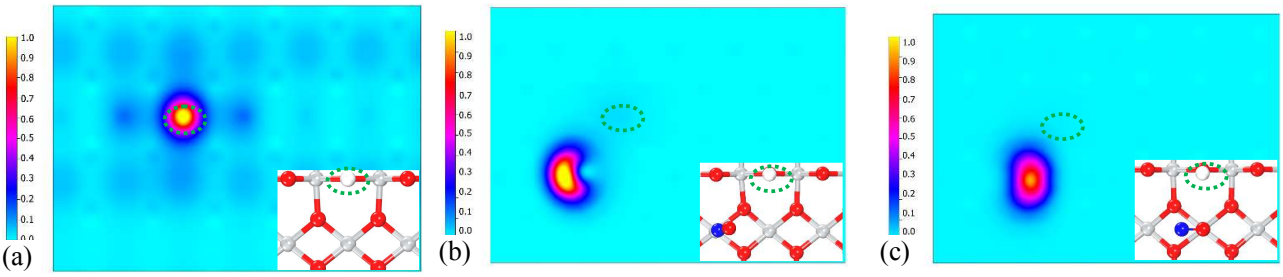

Fig. 5 Simulated STM images of (a) the hydroxylated rutile TiO_2(110) surface, (b) NO adsorbed at the second-nearest Ti atom on (a); (c) intermediate states of NO diffusion on (a). The insets show the corresponding calculated structures in top view. For (a), it is 3.6 Å above Ti_{5c}, at highest density of 3.5×10^{-4} e/Å^3; while for (b-c), it is 5.4 Å above Ti_{5c} atoms，at constant highest density (4.2×10^{-3} e/Å^3).

As mentioned in the above[20], characteristic "bright-dark-bright" (BDB) STM features were observed after NO was dosed on a hydroxylated rutile TiO_2(110) surface. Interestingly, the BDB configuration involves the same three adjacent Ti_{5c} atoms as those in diffusion Pathway I. In order to better understand this relationship, we have simulated STM images (see Fig. 5) within Tersoff−Hamann's approach[37-39] in the constant height mode. An empty-state window of 1.5 eV above the edge of the conduction band was employed. Consistent with the STM results[20], the Ti_{5c} and OH group are visible in Fig. 5(a). After NO adsorbs on the second-nearest Ti atom to the left of the OH group, it appears as a bright, ring-shaped spot (see Fig. 5(b)). While diffusing and changing its configuration to O-end down in the intermediate state, the NO-related spot has a reduced intensity (see Fig. 5(c)). Finally, when it arrives the second-nearest Ti_{5c} atom to the right of the OH, it will recover the original brightness. It should also be noted that, as we can see from the calculated energetics in Fig. 3, these metastable intermediate states give rise to very shallow minima in the potential energy profile, thus their lifetime is expected to be rather short at room temperature. Therefore, they may actually not be seen in STM images, and appear as dark spots. In other words, the diffusion of NO indeed undergoes a typical "bright-dark-bright" process, just as the featured configuration observed in experimental STM images. We can then propose that NO diffusion (Pathway I) on hydroxylated rutile TiO_2(110) surface is the origin of the characteristic BDB configuration observed by STM. It needs to be mentioned that there may exists tip-induced flipping back-and-forth, the tip may lower activation barriers and induce the diffusion. Moreover, as recently demonstrated by Setvin *et al.*[40], tip-surface interaction can change the image contrast of adsorbates quite dramatically. Accordingly, such interaction can be affected in the tip-induced surface process and further reflected in the STM features.

Conclusions

In summary, we have provided theoretical evidence that NO adsorbs on a hydroxylated rutile TiO_2(110) surface by incorporating the excess electron stemming from the OH group on its 2π* anti-bonding orbital. Adsorbed NO can readily diffuse
through an "ON" intermediate state with an O-end down configuration. The diffusion process involves three neighboring Ti_{5c} atoms, namely the left and right second-nearest and the first-nearest middle ones besides the OH group. During the migration, NO also forms a bridge species to maintain its adsorption on the surface. Moreover, this diffusion process appears to be the origin of the characteristic "bright-dark-bright" (BDB) configuration we reported before. These results should be valuable for the interpretation of surface adsorption and diffusion pathways of adsorbates as well as other surface chemistry on rutile TiO_2 and other oxides.

Acknowledgements

The authors thank the financial support from National Basic Research Program (2011CB808505), National Natural Science Foundation of China (21421004, 21322307) and "Shu Guang" project of Shanghai Municipal Education Commission and Shanghai Education Development Foundation (13SG30). UD acknowledges financial support from the ERC Advanced Grant 'OxideSurfaces'. The authors also gratefully acknowledge computing time in the National Super Computing Center in Jinan.

Notes and references

1 W. Zhang, Z. Li, B. Wang and J. Yang, *Int. J. Quantum Chem.*, 2013, **113**, 89-95.
2 C. Sánchez-Sánchez, M. G. Garnier and P. Aebi, et al., *Surf. Sci.*, 2013, **608**, 92-96.

3 Z. Dohnálek, I. Lyubinetsky and R. Rousseau, *Prog. Surf. Sci.*, 2010, **85**, 161-205.
4 C. L. Pang, R. Lindsay and G. Thornton, *Chem. Soc. Rev.*, 2008, **37**, 2328-2353.
5 X. Q. Gong, A. Selloni, M. Batzill and U. Diebold, *Nat. Mater.*, 2006, **5**, 665-670.
6 H. Xu and S. Y. Tong, *Surf. Sci.*, 2013, **610**, 33-41.
7 B. J. Morgan and G. W. Watson, *Surf. Sci.*, 2007, **601**, 5034-5041.
8 Y. Wang, D. Pillay and G. Hwang, *Phys. Rev. B*, 2004, **70**, 193410(1-4).
9 Y. Zhao, Z. Wang, and X.F. Cui, et al., *J. Phys. Chem. C* 2010, **114**, 18222–18227.
10 Z. Wang, Y. Zhao, and J. Hou, et al., *J. Am. Chem. Soc.*, 2009, **131**, 7958-7959.
11 M. Bowker and R. A. Bennett, *J. Phys.: Condens. Matter*, 2010, **22**, 059801-059801.
12 K. Park, M. Pan, V. Meunier and E. Plummer, *Phys. Rev. B*, 2007, **75**, 245415-245422.
13 Z. Zhang, and J. Yates, Jr., et al., *J. Phys. Chem. C*, 2010, **114** 3059–3062.
14 Y.-Y. Yu and X.-Q. Gong, *ACS Catal.*, 2015, **5**, 2042-2050.
15 M. R. Hoffmann, S. T. Martin, W. Choi, and D. W. Bahnemann, *Chem. Rev.*, 1995, **95**, 69-96.
16 A. Fujishimal, T. N. Rao, and D. A. Tryk, *J. Photochem. Photobio. C: Photochem. Rev., 1*, 2000, 1-21.
17 C. Di Valentin, G. Pacchioni and A. Selloni, *Phys. Rev. Lett.*, 2006, **97**, 166803(1-4).
18 A. Shiotari, S. Hatta, H. Okuyama and T. Aruga, *Chem. Sci.*, 2014, **5**, 922-926.
19 J. Zhang, X. Q. Gong and G. Lu, *Phys. Chem. Chem. Phys.*, 2014, **16**, 16904-16908.
20 S.-C. Li, P. Jacobson, S.-L. Zhao, X.-Q. Gong and U. Diebold, *J. Phys. Chem. C*, 2012, **116**, 1887-1891.
21 G. Kresse, J. Furthmüller, *Comput. Mater. Sci.,* 1996, **6** 15-50.
22 G. Kresse, J. Furthmüller, *Phys. Rev. B*, 1996, **54**, 11169-11186.
23 J. P. Perdew, K. Burk, M. Ernzerhof, *Phys. Rev. Lett.*, 1996, **77**, 3865-3868.
24 G. Kresse, D. Joubert, *Phys. Rev. B*, 1999, **56**, 1758-1775.
25 P. E. Blöchl, *Phys. Rev. B*, 1994, **50**, 17953-17979.
26 S. L. Dudarev, G. A. Botton, S. Y. Savrasov, C. J. Humphreys, and A. P. Sutton, *Phys. Rev. B*, 1998, **57**, 1505-1509.
27 V. I. Anisimov, F. Aryasetiawan, A. I. Lichtenstein, *J. Phys.: Condens. Matter,* 1997, **9**, 767–808.
28 S. Grimme, *J. Comput. Chem.*, 2006, **27**, 1787-1799.
29 S. Grimme, *J. Comput. Chem.*, 2004, **25**, 1463-1473.
30 M. Setvin, C. Franchini, and X. Hao, et al., *Phys. Rev. Lett.*, 2014, **113**, 086402.
31 G. Henkelman, B. P. Uberuaga and H. Jónsson, *J. Chem. Phys.*, 2000, **113**, 9901-9904.
32 G. Henkelman and H. Jónsson, *J. Chem. Phys.*, 2000, **113**, 9978-9985.
33 N. A. Deskins, R. Rousseau, and M. Dupuis, *J. Phys. Chem. Lett.*, 2009, **113**, 14583–14586.
34 D. C. Sorescu, C. N. Rusu, and J. T. Yates, Jr., *J. Phys. Chem. B* 2000, **104**, 4408-4417.
35 L. M. Liu, B. McAllister, H. Q. Ye, and P. Hu, *J. Am. Chem. Soc.*, 2006, **128**, 4017-4022.
36 P. Ganesh, P. R. C. Kent and G. M. Veith, *J. Phys. Chem. Lett.*, 2011, **2**, 2918-2924.
37 G. Teobaldi, W. A. Hofer, O. Bikondoa, C. L. Pang, G. Cabailh and G. Thornton, *Chem. Phys. Lett.*, 2007, **437**, 73-78.
38 J. Tersoff and D. R. Hamann, *Phys. Rev. B*, 1985, **31**, 805-813.
39 J. Bardeen, *Phys. Rev. Lett.*, 1961, **6**, 57-59.
40 M. Setvin, B. Daniel, and U. Aschauer, et al., *Phys. Chem. Chem. Phys.*, 2014, **16**, 21524-21530.